Journal of Materials Chemistry

Cite this: *J. Mater. Chem.*, 2011, **21**, 11253

www.rsc.org/materials

PAPER

Synthesis of novel hierarchical graphene/polypyrrole nanosheet composites and their superior electrochemical performance†

Chaohe Xu, Jing Sun* and Lian Gao*

Received 25th March 2011, Accepted 19th May 2011
DOI: 10.1039/c1jm11275a

Novel hierarchical graphene/polypyrrole (GNS/PPy) nanosheet composites have been successfully fabricated for the first time based on an *in situ* chemical oxidation polymerization method. Sheet-like PPy with a thickness of 20–50 nm grown on the surface of the composites of the GNS/PPy polymerized at an early stage due to the dominated role of the sheet-like GNS and residue glucose in the synthesis process. Supercapacitors based on the hierarchical composite exhibit large electrochemical capacitance (318.6 F g^{-1}) at a scan rate of 2 mV s^{-1}. They also show superior electrochemical rate capability and cyclic stability. The capacitance retained ~95% (132.9 F g^{-1}) after 1000 cycles at a scan rate of 100 mV s^{-1}. Accordingly, the hierarchical GNS/PPy nanosheet composites are potential electrode materials for electrochemical supercapacitors.

Introduction

Over the past decades, supercapacitors have attracted significant attention due to their higher power density, longer cycle life than batteries and higher energy density than conventional capacitors,[1–4] which make them potential candidates for hybrid electric vehicles, short-term power sources for mobile electronic devices and other renewable energy storage applications.

Nowadays, many researches on electrochemical capacitors aim at increasing power and energy density as well as lowering fabrication costs. RuO_2 and its composites show prominent properties as pseudocapacitive electrode materials; however, the high cost excludes it from many applications.[5,6] Therefore, low cost electrode materials have been intensively investigated as electrode materials for supercapacitors in recent years.[2,7–9] Among these materials, conducting polymers (CPs) have been considered as one of the most promising electrode materials for redox supercapacitors due to its ease of synthesis and high conductivity. However, their capacitance value and cycling stability are much lower than that of RuO_2.[1] Carbon nanomaterials, such as mesoporous carbon and carbon nanotubes (CNTs), have attracted considerable interest owing to their good stability as electrodes for supercapacitors. However, the capacitance values are limited by their microstructures.[10] Therefore, composite materials incorporated with the above two components have been achieved due to the synergetic effects.[1,11,12] Core-shell structures of CNT/PANi and CNT/PPy have been prepared and show enhanced electrochemical properties.[13,14] CNT/PPy hybrid films with controlled pore sizes have also been successfully fabricated and exhibited a specific capacitance of 250 F g^{-1} at a scan rate 10 mV s^{-1}.[15] The superior electrochemical properties of CNT/CP composites are mainly ascribed to the strong π–π stacking interaction between the conjugated backbones of the CPs and the graphitic sidewalls of MWCNTs which are beneficial to the electron transportation.[16]

Recently, graphene nanosheets (GNS), two-dimensional carbon nanomaterials, have received significant research attention in energy storage devices due to the unique electronic, mechanical properties and large surface areas.[17] Chemically modified GNS, which has high conductivity, high surface area and good mechanical properties, comparable with or even better than that of CNTs can be prepared by facile wet method.[18–20] In addition, the composites of GNS can be obtained through simple chemical procedures, such as *in situ* chemical or electrochemical polymerization and noncovalent functionalization.[21–23] Therefore, the potential of using GNS-based composites, especially for GNS/CP composites, has attracted much attention as electrode materials for supercapacitors.[22,24,25] Specific capacitance as high as 480 F g^{-1} has been achieved over PANi-doped GNS composites and revealed good cycling stability.[10] Flexible GNS/PANi nanofibers hybrid films prepared by vacuum filtration exhibited large electrochemical capacitance of 210 F g^{-1} at a current density of 0.3 A g^{-1}.[26] Although the GNS/CP composites have been investigated extensively as electrode materials for supercapacitors, there are few reports on constructing hierarchical composites by combining two-dimensional GNS and CP nanosheets together. Furthermore, the hierarchical composites can provide more electrochemical active sites and short distances for ion and electron transporting for electrode materials, due to their large contact area with the electrolyte.[27]

The State Key Lab of High Performance Ceramics and Superfine Microstructure, Shanghai Institute of Ceramics, Chinese Academy of Sciences, 1295 Ding Xi Road, Shanghai, 200050, China. E-mail: jingsun@mail.sic.ac.cn; liangao@mail.sic.ac.cn; Fax: +86 21 52413122; Tel: +86 21 52414301

† Electronic supplementary information (ESI) available. See DOI: 10.1039/c1jm11275a

Moreover, controlling the thickness of materials on an appropriate level is beneficial to improve the electrochemical properties due to the interface electrochemical behavior for supercapacitors.

Herein, we report an ultrathin hierarchical GNS/PPy nanosheet composite as electrode materials for supercapacitors by an *in situ* chemical polymerization method. The as prepared hierarchical GNS/PPy nanosheet composites show superior electrochemical properties compared with previous results.[15,28] Therefore, such hierarchical GNS/PPy nanosheet composites will be potential electrode materials for supercapacitors.

Experimental section

Materials

Graphite (-325 mesh) was purchased from Alfa Aesar. All chemicals were of analytical grade and used without further purification.

Synthesis of graphene oxide (GO)

GO was prepared from graphite flakes by the modified Hummers method. 1.0 g of graphite flakes, 1.0 g of $NaNO_3$ and 46 mL of concentrated H_2SO_4 were mixed together in an ice bath for 4 h. Then 6.0 g of $KMnO_4$ were added slowly into the solution. Afterwards, the ice bath was removed and the suspension was stirred for another 2 days. After adding 100 mL of distilled water dropwise, the suspension was heated in oil bath at 98 °C for 30 min. Then the suspension was further treated with 200 mL of warm water (~60 °C) and 10 mL of H_2O_2 (30%). The mixture was centrifuged at 4000 rpm and washed with diluted HCl and water to neutral. Finally, a homogeneous GO aqueous dispersion (0.2 mg mL^{-1}) was obtained for further using.

Synthesis of hierarchical GNS/PPy nanosheet composite

The GNS obtained by a green and facile approach reported by Dong and coworkers.[29] Briefly, 200 mg glucose was added into the above GO suspension, followed by stirring for 30 min. Then, 100 μL of ammonia solution (25–28%) were added into the resulting dispersion. The mixture was stirred for 90 min at 95 °C. After centrifugation and washing with water and ethanol several times, the obtained GNS was redispersed in 100 mL deionized water by bath-sonication for 30 min. Then, 25, 50, 75, 100, 125, 150 and 200 μL of pyrrole were added into the redispersed GNS suspension, followed by stirring for more than 30 min. The products were marked as GNS-PPy-M (M is the volume of pyrrole). Afterwards, 0.1 mL of concentrated HCl was added into the above suspension and sonicated for another 5 min. Then, 5 mL of ammonium persulfate (APS, 1 mmol) aqueous solution were added into the above reaction system and kept at 0–4 °C for 4–6 h. Finally, the obtained GNS/PPy nanosheet composite was washed with distilled water and ethanol, and dried in a vacuum oven at 60 °C for 24 h. The pure PPy were also prepared by the chemical oxidation polymerization process above.

Characterization methods

Transmission electron microscopy (TEM) was performed on a JEM-2100F Electron Microscope with an accelerating voltage of 200 kV. Field-emission scanning electron microscopy (FE-SEM) was performed on a JSM-6700F at an acceleration voltage of 10.0 kV. FT-IR and Raman spectroscopy were recorded on a Nicolet 7000-C and DXR Raman Microscope with 532 nm excitation length, Thermal Scientific Co., USA, respectively.

In the electrochemical test, the active electrode was assembled into a three-electrode cell system. The electrode was prepared according to the following steps. The mixture containing 5 mg of active materials and 5 mg of polyvinylidene fluoride (PVDF) binder was well mixed, and then 1 mL of absolute ethanol was added to the mixtures and sonicated for 1 h to obtain a homogeneous suspension. Then, 10 μL of the as prepared suspension was dropped onto the glassy carbon electrode and dried in an oven before the electrochemical test (the loading amount of active materials is 50 μg). The used electrolyte was 1 M H_2SO_4 solution. The electrochemical behavior was characterized within a potential window of −0.1 to 0.5 V *vs.* SCE reference electrode. Platinum wire was used as a counter electrode. All the electrochemical experiments were carried out using a Parstat 2273 electrochemical station (Princeton applied research CO., Ltd, USA).

Results and discussion

Microstructure characterizations

Fig. 1a shows a typical transmission electron microscopy (TEM) image of the as synthesized graphene oxides (GO) which were prepared by the modified Hummers method.[30] From the TEM image, we can observe that most GO are of single to a few layers thick and stacked together. The inset of Fig. 1a is the corresponding selected area electron diffraction (SAED) pattern of the as prepared GO. Individual spots are not visible as the contributing patterns merge into rings, which is characteristic of

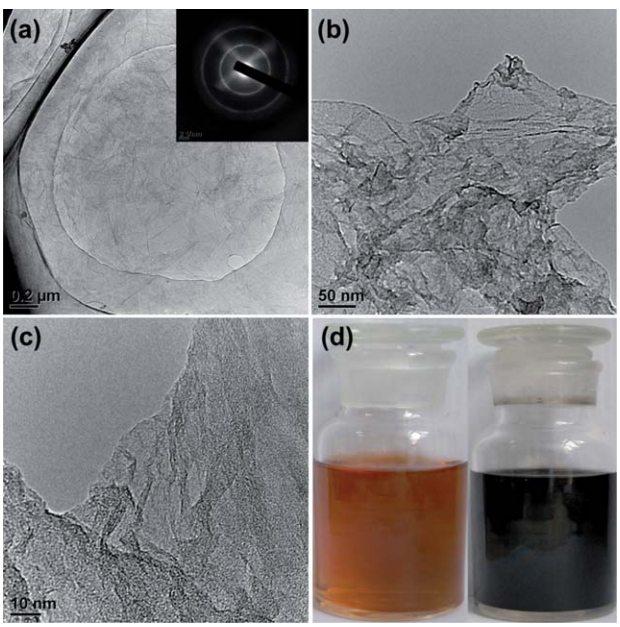

Fig. 1 Typical TEM images of the as-synthesized graphene at different magnifications.

polycrystalline samples. This suggests that no preferred stacking orientations exist in GNS.[31] The typical low and high magnification TEM images of GNS are shown in Fig. 1b–c. As shown in Fig. 1b, the GNS are very thin and stacked together. The high magnification TEM image (Fig. 1c) clearly shows the stacking layers at the edges of the GNS. Fig. 1d shows the optical image of aqueous dispersions (0.2 mg mL^{-1}) of GO before and after reduction. The obtained GNS are uniformly dispersed in aqueous solution and appeared as a homogeneous suspension, which can be stably dispersed in water for more than one month. This can be attributed to glucose that may also play a role as a capping reagent to stabilize the GNS suspension.[29,32,33]

TEM images of the as prepared hierarchical GNS/PPy nanosheet composites are shown in Fig. 2. The samples with a similar microstructure aggregated together (Fig. 2a, c and d). Fig. 2b is the high magnification TEM image of the sample GNS-PPy-50, from which we can see that the thin layers of PPy are coated on the surfaces of GNS. The GNS/PPy composites are formed owing to the strong π–π stacking interaction between the 2D monolayer of sp^2-bonded carbon atoms and the electronic structures of the conjugated backbones of PPy. Briefly, pyrrole monomers were firstly adsorbed onto the surface of GNS *via* π–π interactions, hydrogen bonds and Van der Waals forces (Scheme 1). Then, the oxidant of APS was introduced and PPy layers formed and coated the surface of the GNS during the *in situ* chemical oxidation polymerization process. Fig. 3 shows the Fourier transformation infrared (FTIR) spectrum of PPy and GNS-PPy composites. For sample GNS-PPy-100, the bands at 1557 and 1465 cm^{-1} may be assigned to typical PPy ring vibrations, and the band at 1295 cm^{-1} corresponds to =C–H band in-plane vibrations. The peak at 1184 cm^{-1} is assigned to the N–C stretching vibration and the bands at 789, 963 cm^{-1} verify the presence of polymerized pyrrole. The FT-IR peak observed at

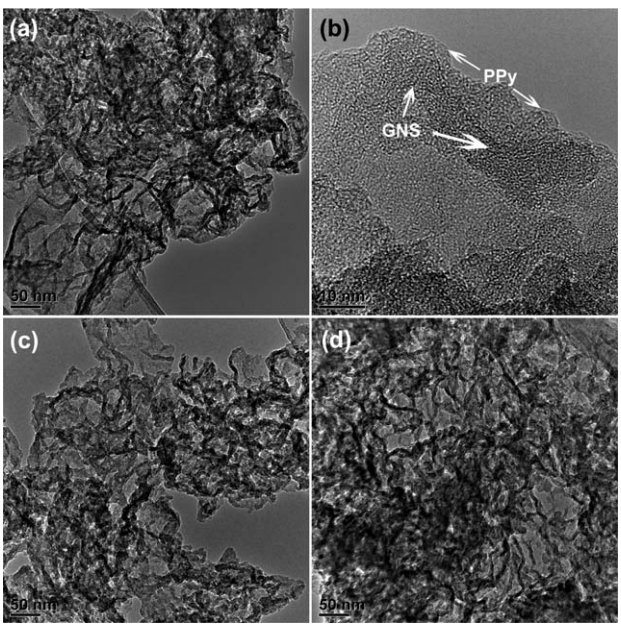

Fig. 2 TEM images of the graphene/polypyrrole nanosheet composites. (a, b) Low- and high-magnifications TEM images of sample GNS-PPy-50; (c) GNS-PPy-75; (d) GNS-PPy-100.

Scheme 1 *In situ* chemical oxidation polymerization mechanism of polypyrrole on graphene.

901 cm^{-1} may be assigned to the =C–H out of plane vibration indicating the polymerization of pyrrole.[34] The spectrum of samples also exhibits the presence of some residue oxide groups, such as O–H at 3400 cm^{-1} and C–O at 1070 cm^{-1}, which can act as active sites for nucleation.[23,29,35] These vibrations are all reflected in the spectra of pure PPy, GNS-PPy-50 and GNS-PPy-75 (curves (a) to (c) in Fig. 3). Raman spectrum of the nanosheet composites are shown in Figure S1 (supporting information).† Raman shifts occurred for the G band of GNS/PPy composites (1578 cm^{-1}) compared with that of GNS (1590 cm^{-1}) due to the strong π–π interactions of PPy and GNS;[29,36] the peak at 1103 cm^{-1} may be assigned to the quinonoid bipolaronic structure.[37–39] The G bands of GNS-PPy composites shifted to lower frequency because of the electron-donating effect of the substituent of benzene group (n-type doping effect).[40,41] These are similar to the effects of molecular charge-transfer with donor and acceptor molecules.[40] Therefore, it can be deduced that the GNS are covered by PPy, and there are interactions (probably π–π noncovalent bonds) between PPy and GNS.[42]

Typical field-emission scanning electron microscopy (FE-SEM) images of the hierarchical GNS/PPy nanosheet composites are shown in Fig. 4. The GNS/PPy composites have a rough surface as shown in Fig. 4a. The PPy was formed and fixed to the surface of GNS after polymerization. PPy nanosheets with a thickness of 20–50 nm are also observed in the GNS/PPy composites. When the volume of pyrrole increased to 75 μL (Fig. 4b, sample GNS-PPy-75), the amount of PPy nanosheets remarkably increased and were uniformly distributed on the surface of the GNS/PPy composites. For sample GNS-PPy-100, the GNS/PPy composites are fully coated by PPy nanosheets

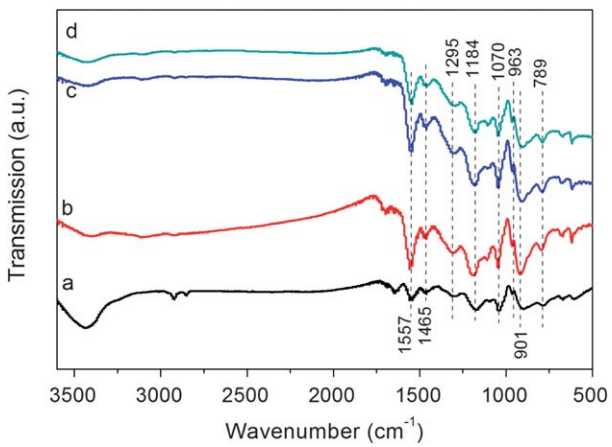

Fig. 3 FTIR spectra of the graphene/polypyrrole nanosheet composites, (a) polypyrrole; (b) GNS-PPy-50; (c) GNS-PPy-75; (d) GNS-PPy-100.

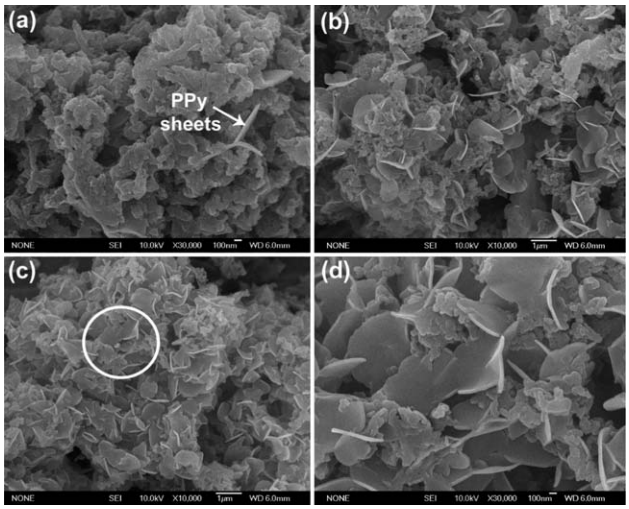

Fig. 4 FE-SEM images of the graphene/polypyrrole nanosheet composites. (a) GNS-PPy-50. (b) GNS-PPy-75. (c, d) Low- and high-magnifications FE-SEM images of sample GNS-PPy-100.

with diameters of 1.0 to 1.5 μm. The thicknesses of the PPy nanosheets remained ~20–50 nm when the concentration of pyrrole varied from 50 to 100 μL. Based on these, a possible formation mechanism for the hierarchical GNS/PPy nanosheet composites is proposed in Scheme 2. First, pyrrole monomers were adsorbed onto the larger surface of GNS *via* π–π interactions, hydrogen bonds and Van der Waals forces. With the addition of APS aqueous solution, the chemical polymerization occurred and formed GNS/PPy composites with a rough surface (typical example is the sample GNS-PPy-25, Figure S2b†). The SEM image of the obtained GNS with a uniform surface is shown in Figure S2a.† The GNS are very large and all aggregate together. As the volume of pyrrole increased to 75 μL, sheet-like PPy grew on the surface of the GNS/PPy composites and formed hierarchical structures (Fig. 4b and step 2 in Scheme 2). Increasing the pyrrole volume further to 100 or 125 μL resulted in more PPy nanosheets (Fig. 4c,d and Figure S3a,† step 3 in Scheme 2). The hierarchical structures provide a larger surface area for the electrochemical reaction, which indicates superior electrochemical performance. When the volume of pyrrole was increased to 150 and 200 μL (Figure S3b–d†), the PPy nanosheets embedded into PPy nanoparticles (Figure S3b-c); and will disappear completely when continuing to increase the volume of pyrrole (Figure S3d). The contents of PPy are 88.3, 89.7, 90.8, 92, 93.7 and 95.1% for the obtained GNS-PPy composites, respectively.

To prove the formation process of the hierarchical nanosheet composites, sample GNS-PPy-100 was taken out during the polymerization process at different time intervals (Fig. 5a-c). The GNS-PPy composites with rough surface were formed after 30 min of polymerization (Fig. 5a) compared with GNS (Figure S2a†), indicating the formation of PPy. The residue functional groups on GNS acted as active sites and enabled the *in situ* polymerization of PPy;[35] the π–π stacking force was beneficial to the chemical reaction occurred on the surface of GNS. Sheet-like PPy appeared on the surface of the composites after 1 h of chemical polymerization (Fig. 5b), which verified that they were formed on the surface of previously polymerized GNS-PPy composites at an early stage. After 2 h of polymerization, more and more PPy sheets appeared and gradually grew (Fig. 5c). In order to understand the role of GNS in the formation of GNS/PPy nanosheet composites, pure PPy was synthesized for comparison (Fig. 5d). As displayed in Fig. 5d, sphere-like particles with diameters of 400–600 nm are clearly observed, which is totally different from the sheet-like shape with the presence of GNS. When GO was reduced without glucose, there were no PPy nanosheets observed in the GNS/PPy composites (Figure S4a†). As a comparison, we found that glucose has no impact on the morphology of pure PPy nanoparticles, in which sphere-like PPy particles with diameters of 300–500 nm are observed (Figure S4b†). Therefore, it can be concluded that the GNS and residue glucose on GNS play the dominated role in the formation of PPy nanosheets.

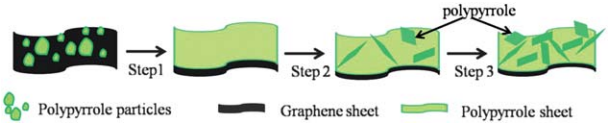

Scheme 2 The formation mechanism for GNS-PPy nanosheet composites.

Electrochemical analysis

Fig. 6a–c show the cyclic voltammetry (CV) curves of the GNS/PPy nanosheet composites at different scan rates in 1 M H_2SO_4 aqueous solution. The specific capacitance of the electrodes was calculated from the CV results according to the following equation,[43]

$$C_m = \frac{1}{v(V_c - V_a)} \int_{V_a}^{V_c} I(V)\mathrm{d}V \quad (1)$$

where C_m is the specific capacitance, v is the potential scan rate (mV s^{-1}), $V_c - V_a$ represents the sweep potential range and $I(V)$

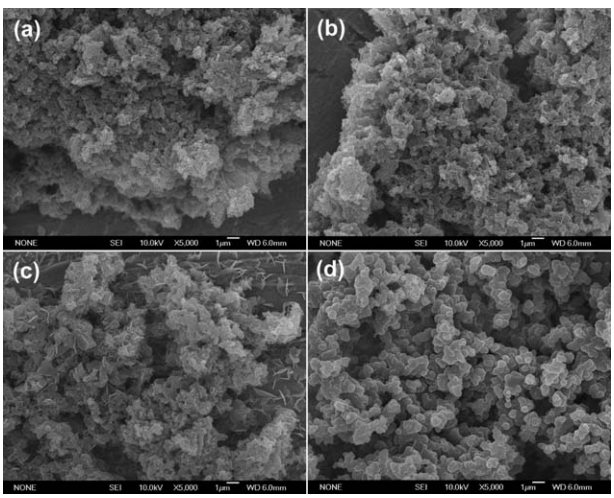

Fig. 5 SEM images of GNS-PPy samples obtained at different reaction intervals: (a) 30 min, (b) 1 h, (c) 2 h and (d) pure PPy.

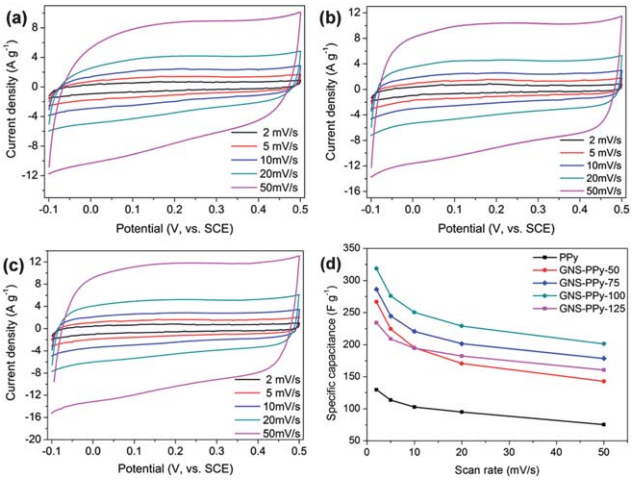

Fig. 6 CV curves of hierarchical GNS/PPy nanosheet composites at various scan rates. (a) GNS-PPy-50. (b) GNS-PPy-75. (c) GNS-PPy-100. (d) The variation of the specific capacitance of GNS/PPy nanosheet composites at different scan rates.

denote the response current density (A g^{-1}). Rectangular shapes of the CV curves, which are the response of an ideal capacitor, are found for the GNS/PPy electrodes when the scan rate is lower than 50 mV s^{-1} (Fig. 6a–c). These indicate that the composites exhibit a double layer electric capacitive behavior. The CV curves at a scan rate of 50 mV s^{-1} are not rectangular and opened at the low-voltage side due to polarization of the electrodes. At higher scan rates, the concentration of ions on the solid/liquid interface increase rapidly and the diffusion rate of electrolyte from solid/liquid interface to electrode materials is not fast enough to satisfy the electrochemical reactions of electrode materials. These result in the enrichment of electrolyte near the solid/liquid interface and polarization of the electrode materials. The variations of their specific capacitance as a function of scan rates are plotted in Fig. 6d. The specific capacitances are 266.7, 286.3 and 318.6 F g^{-1} for samples GNS-PPy-50, GNS-PPy-75 and GNS-PPy-100 at 2 mV s^{-1}, respectively, which are superior to that of the composites of GNS/PANI[21,26] and CNT/PPy.[16,44] By further increasing the scan rate to 50 mV s^{-1}, the specific capacitances are still as high as 142.9, 178.6 and 201.4 F g^{-1} for the three samples. For GNS-PPy-125 and pure PPy nanoparticles (Figure S5†), the specific capacitances are 234.3 and 129.9 F g^{-1} at 2 mV s^{-1}, respectively. The detailed results of the initial specific capacitance of the hierarchical GNS/PPy nanosheet composites are shown in Table 1. Sample GNS-PPy-125 has relatively low electrochemical properties compared with GNS-PPy-100. It can be attributed to the fact that the extra formed PPy are not closely combined with GNS. Therefore, the electron transportation between PPy and GNS is inferior to PPy nanosheets formed at the early stage. These will lead to a lower contribution to the specific capacitance of the composites. However, the GNS/PPy nanosheet composites have superior electrochemical performance than that of pure PPy nanoparticles owing to the synergetic effects between GNS and PPy.

Due to its highest specific capacitance, GNS-PPy-100 was selected for further investigation. The CV curves of sample GNS-PPy-100 at high scan rates are shown in Fig. 7a. The initial specific capacitance calculated at 100, 200, 500 and 1000 mV s^{-1} is 139.2, 100, 68 and 41.9 F g^{-1}, respectively. They maintain rectangular shape with only small distortions even at 200 mV s^{-1}. The sample exhibited enhanced rate capability than the previous reported results of PPy or GNS composites.[23,44,45] The larger surface areas and ultrathin sheet-like PPy nanostructure in the present work not only provide more electrochemically active sites but also shorten the distance for ion and electron transportation.

The electrochemical stability of GNS-PPy-100 was also investigated in the range of −0.1–0.5 V at a scan rate of 100 mV s^{-1}. It is found that the GNS-PPy-100 electrode retained ~95% (132.9 F g^{-1}) of the initial capacitance after 1000 cycles (Fig. 7b). As it is well known, double-layer capacitors have a better electrochemical stability than pseudocapacitators.[46] The PPy electrodes are mostly related to a redox reaction which belongs to pseudocapacitance.[28,47,48] Graphene has good electrochemical double layer performance and superior electron transportation properties,[20] so it can provide enough electrons for electrochemical reactions of PPy nanosheets. Based on their specific microstructures and their intrinsic electrochemical properties of the two components, the hierarchical GNS/PPy nanosheet composites exhibit superior electrochemical stability and can be applied as electrode materials for electrochemical supercapacitors.

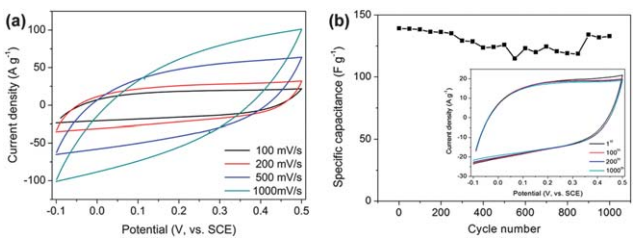

Fig. 7 (a) CV curves of sample GNS-PPy-100 at scan rates of 100, 200, 500 and 1000 mV s^{-1}. (b) Cycle life of sample GNS-PPy-100 at 100 mV s^{-1} in 1 M H_2SO_4 solution. Inset in (b) is the CV curves of the 1st to 1000th cycles of sample GNS-PPy-100.

Table 1 The specific capacitances of the GNS/PPy composites at different scan rates

Scan rate (mV s^{-1})	Polypyrrole (F g^{-1})	GNS-PPy-50 (F g^{-1})	GNS-PPy-75 (F g^{-1})	GNS-PPy-100 (F g^{-1})	GNS-PPy-125 (F g^{-1})
2	129.9	266.7	286.3	318.6	234.3
5	113.6	224.5	244.7	276.1	208.8
10	102.7	195.3	220.6	250.5	244.7
20	94.9	170.7	201.6	229.1	182.4
50	75.5	142.9	178.6	201.4	160.6

Conclusions

The novel hierarchical GNS/PPy nanosheet composites have been prepared *via* a simple *in situ* chemical oxidation polymerization procedure. The PPy nanosheets with thickness of 20–50 nm can be synthesized on GNS/PPy composites by adjusting the concentration of the pyrrole. The formation of the structure is due to the presence of the sheet-like GNS in the synthesis process. Supercapacitors based on these hierarchical composites exhibited good electrochemical capacitance as high as 318.6 F g^{-1} at a scan rate of 2 mV s^{-1}. They also showed superior electrochemical rate capability and cyclic stability. It retained ~95% (132.9 F g^{-1}) of the initial capacitance after 1000 cycles at a scan rate of 100 mV s^{-1}. The large surface areas and short electron transportation distance contribute to the high performance. Therefore, the hierarchical GNS/PPy nanosheet composites will be a promising electrode material for electrochemical supercapacitors.

Acknowledgements

This work is supported by the National Natural Science Foundation of China (NO. 50972153).

References

1 Y. G. Wang, H. Q. Li and Y. Y. Xia, *Adv. Mater.*, 2006, **18**, 2619–2623.
2 R. Liu and S. B. Lee, *J. Am. Chem. Soc.*, 2008, **130**, 2942–2943.
3 H. Zhang, G. P. Cao, Z. Y. Wang, Y. S. Yang, Z. J. Shi and Z. N. Gu, *Nano Lett.*, 2008, **8**, 2664–2668.
4 H. J. Liu, L. H. Jin, P. He, C. X. Wang and Y. Y. Xia, *Chem. Commun.*, 2009, 6813–6815.
5 Y. Wang, C. Y. Foo, T. K. Hoo, M. Ng and J. Y. Lin, *Chem.–Eur. J.*, 2010, **16**, 3598–3603.
6 B. Gao, L. Hao, Q. B. Fu, L. H. Su, C. Z. Yuan and X. G. Zhang, *Electrochim. Acta*, 2010, **55**, 3681–3686.
7 K. H. An, W. S. Kim, Y. S. Park, J. M. Moon, D. J. Bae, S. C. Lim, Y. S. Lee and Y. H. Lee, *Adv. Funct. Mater.*, 2001, **11**, 387–392.
8 C. J. Yu, C. Masarapu, J. P. Rong, B. Q. Wei and H. Q. Jiang, *Adv. Mater.*, 2009, **21**, 4793–4797.
9 Y. Wang, Y. Wan and D. Zhang, *Electrochem. Commun.*, 2010, **12**, 187–190.
10 K. Zhang, L. L. Zhang, X. S. Zhao and J. S. Wu, *Chem. Mater.*, 2010, **22**, 1392–1401.
11 J. E. Huang, X. H. Li, J. C. Xu and H. L. Li, *Carbon*, 2003, **41**, 2731–2736.
12 Y. K. Zhou, B. L. He, W. J. Zhou, J. Huang, X. H. Li, B. Wu and H. I. Li, *Electrochim. Acta*, 2004, **49**, 257–262.
13 L. Li, Z. Y. Qin, X. Liang, Q. Q. Fan, Y. Q. Lu, W. H. Wu and M. F. Zhu, *J. Phys. Chem. C*, 2009, **113**, 5502–5507.
14 Y. J. Yu, O. Y. Chu, Y. Gao, Z. H. Si, W. Chen, Z. Q. Wang and G. Xue, *J. Polym. Sci., Part A: Polym. Chem.*, 2005, **43**, 6105–6115.
15 J. Y. Kim, K. H. Kim and K. B. Kim, *J. Power Sources*, 2008, **176**, 396–402.
16 Y. P. Fang, J. W. Liu, D. J. Yu, J. P. Wicksted, K. Kalkan, C. O. Topal, B. N. Flanders, J. D. Wu and J. Li, *J. Power Sources*, 2010, **195**, 674–679.
17 K. S. Kim, Y. Zhao, H. Jang, S. Y. Lee, J. M. Kim, J. H. Ahn, P. Kim, J. Y. Choi and B. H. Hong, *Nature*, 2009, **457**, 706–710.
18 D. H. Wang, R. Kou, D. Choi, Z. G. Yang, Z. M. Nie, J. Li, L. V. Saraf, D. H. Hu, J. G. Zhang, G. L. Graff, J. Liu, M. A. Pope and I. A. Aksay, *ACS Nano*, 2010, **4**, 1587–1595.
19 S. Q. Chen and Y. Wang, *J. Mater. Chem.*, 2010, **20**, 9735–9739.
20 M. D. Stoller, S. J. Park, Y. W. Zhu, J. H. An and R. S. Ruoff, *Nano Lett.*, 2008, **8**, 3498–3502.
21 D. W. Wang, F. Li, J. P. Zhao, W. C. Ren, Z. G. Chen, J. Tan, Z. S. Wu, I. Gentle, G. Q. Lu and H. M. Cheng, *ACS Nano*, 2009, **3**, 1745–1752.
22 H. Bai, Y. X. Xu, L. Zhao, C. Li and G. Q. Shi, *Chem. Commun.*, 2009, 1667–1669.
23 A. V. Murugan, T. Muraliganth and A. Manthiram, *Chem. Mater.*, 2009, **21**, 5004–5006.
24 H. L. Wang, Q. L. Hao, X. J. Yang, L. D. Lu and X. Wang, *Electrochem. Commun.*, 2009, **11**, 1158–1161.
25 H. Wang, Q. Hao, X. Yang, L. Lu and X. Wang, *Nanoscale*, 2010, **2**, 2164–2170.
26 Q. Wu, Y. X. Xu, Z. Y. Yao, A. R. Liu and G. Q. Shi, *ACS Nano*, 2010, **4**, 1963–1970.
27 J. J. Xu, K. Wang, S. Z. Zu, B. H. Han and Z. X. Wei, *ACS Nano*, 2010, **4**, 5019–5026.
28 B. C. Kim, J. M. Ko and G. G. Wallace, *J. Power Sources*, 2008, **177**, 665–668.
29 C. Z. Zhu, S. J. Guo, Y. X. Fang and S. J. Dong, *ACS Nano*, 2010, **4**, 2429–2437.
30 V. C. Tung, M. J. Allen, Y. Yang and R. B. Kaner, *Nat. Nanotechnol.*, 2009, **4**, 25–29.
31 N. R. Wilson, P. A. Pandey, R. Beanland, R. J. Young, I. A. Kinloch, L. Gong, Z. Liu, K. Suenaga, J. P. Rourke, S. J. York and J. Sloan, *ACS Nano*, 2009, **3**, 2547–2556.
32 M. J. Fernandez-Merino, L. Guardia, J. I. Paredes, S. Villar-Rodil, P. Solis-Fernandez, A. Martinez-Alonso and J. M. D. Tascon, *J. Phys. Chem. C*, 2010, **114**, 6426–6432.
33 J. L. Zhang, H. J. Yang, G. X. Shen, P. Cheng, J. Y. Zhang and S. W. Guo, *Chem. Commun.*, 2010, **46**, 1112–1114.
34 V. Selvaraj, M. Alagar and K. S. Kumar, *Appl. Catal., B*, 2007, **75**, 129–138.
35 S. Chen, J. W. Zhu, X. D. Wu, Q. F. Han and X. Wang, *ACS Nano*, 2010, **4**, 2822–2830.
36 K. N. Kudin, B. Ozbas, H. C. Schniepp, R. K. Prud'homme, I. A. Aksay and R. Car, *Nano Lett.*, 2008, **8**, 36–41.
37 S. Demoustier-Champagne and P. Y. Stavaux, *Chem. Mater.*, 1999, **11**, 829–834.
38 Z. S. Wu, W. C. Ren, L. B. Gao, B. L. Liu, C. B. Jiang and H. M. Cheng, *Carbon*, 2009, **47**, 493–499.
39 T. M. Wu, H. L. Chang and Y. W. Lin, *Compos. Sci. Technol.*, 2009, **69**, 639–644.
40 B. Das, R. Voggu, C. S. Rout and C. N. R. Rao, *Chem. Commun.*, 2008, 5155–5157.
41 D. C. Wei, Y. Q. Liu, Y. Wang, H. L. Zhang, L. P. Huang and G. Yu, *Nano Lett.*, 2009, **9**, 1752–1758.
42 H. F. Guo, H. Zhu, H. Y. Lin and J. Q. Zhang, *Colloid Polym. Sci.*, 2008, **286**, 587–591.
43 X. F. Xie and L. Gao, *Carbon*, 2007, **45**, 2365–2373.
44 L. Z. Fan and J. Maier, *Electrochem. Commun.*, 2006, **8**, 937–940.
45 R. K. Sharma, A. C. Rastogi and S. B. Desu, *Electrochem. Commun.*, 2008, **10**, 268–272.
46 M. Winter and R. J. Brodd, *Chem. Rev.*, 2004, **104**, 4245–4269.
47 Q. F. Wu, K. X. He, H. Y. Mi and X. G. Zhang, *Mater. Chem. Phys.*, 2007, **101**, 367–371.
48 J. H. Kim, Y. S. Lee, A. K. Sharma and C. G. Liu, *Electrochim. Acta*, 2006, **52**, 1727–1732.

